JOURNAL OF MATERIALS SCIENCE **33** (1998) 1349–1357

Structural and compositional studies of magnetron-sputtered Nd–Fe–B thin films on Si(100)

G. K. MURALIDHAR, B. WINDOW*, D. K. SOOD, R. B. ZMOOD
Department of Electrical Engineering, Royal Melbourne Institute of Technology, 124, La Trobe Street, Melbourne, Vic. 3001, Australia
**Division of Applied Physics, Commonwealth Scientific and Industrial Research Organization, Lindfield, Sydney, NSW 2070, Australia*
E-mail: murali@rmit.edu.au

The structure and composition of the Nd–Fe–B thin films deposited on Si(100) have been investigated. Films have been prepared by direct-current magnetron sputtering in pure argon and xenon sputter media separately. Deposition has been carried out keeping the substrates at room temperature and 360 °C. These films were subjected to the post-deposition annealing to a temperature of 600 °C in a vacuum of 5×10^{-7} Torr. The stoichiometry and structure of these films were analysed and correlated to the deposition and annealing conditions. Films deposited in xenon sputter medium showed better crystalline properties than those sputtered in pure argon. This difference was attributed to the presence of reflected high-energy neutral gas particles in the argon medium. Films deposited in xenon were found to be relatively rich in boron compared with argon-sputtered films. Post-deposition annealing resulted in the interdiffusion at the interface between the film and substrate. The use of a SiO_2 film as a barrier layer between the silicon substrate and the Nd–Fe–B film has been explored. Thermally grown SiO_2 was found to be an effective diffusion barrier. © *1998 Chapman & Hall*

1. Introduction

Thin films of permanent magnetic materials have continued to be in the centre of an upsurge in research activity with the advent of microengineering of electromechanical systems. The key to the success of such miniaturizing technologies is the development of thin-film magnets with uniaxial anisotropy and high energy products. Another major step in this direction would be the integration of magnetics with the existing silicon technology. There have been a number of reports [1–5] on the sputter deposition of Nd–Fe–B thin films on various substrates such as glass, sapphire, quartz and metals such as niobium and tantalum. These films are either deposited above 600 °C or annealed after deposition to such temperatures. Most of these studies succeeded in achieving good magnetic properties with coercivities as high as 15 kOe and also high energy products. It was found that the crystalline structure, microstructure and magnetic anisotropies could be altered by changing the deposition conditions such as the substrate temperature, operating pressure and deposition rate. For example, at low deposition rates (less than 1.8 Å s^{-1}, Cadieu [6] has grown $Nd_2Fe_{14}B$ thin films by radio-frequency diode sputtering, which can be easily magnetized out of the film plane. At high deposition rates (greater than 1.8 Å s^{-1}), films were found to be easily magnetized in the film plane. Similar observations have been made with respect to the substrate temperature also, i.e., films deposited at a substrate temperature of 600 °C were easier to magnetize perpendicular to the film plane, whereas deposition at substrate temperature of 700 °C led to the formation of films easier to magnetize in the film plane depending on the deposition rate and other conditions. However, the absolute values of these parameters at which the film properties change are considered to be system and geometry dependent. Another interesting aspect of these investigations [6] is the use of high sputtering gas (argon) pressures around 150–200 mTorr so as to thermalize the sputtered atoms. The sputtered atoms with different masses are believed to have thermalized before reaching the substrate at these high operating pressures.

In the present work, the need to integrate these magnetic films with the silicon micro-machining technology has led us to deposit the Nd–Fe–B thin films on Si(100) substrates. Some of the earlier efforts of this group to deposit the films on Si(100) using ion-beam sputtering could produce highly textured films on the substrates kept at room temperature [7]. As it is difficult to deposit thicker films using ion-beam sputtering with its low deposition rates (0.02 nm s^{-1}), direct-current magnetron sputtering was used in the present investigations. The effects of the deposition

 © *1998 Chapman & Hall*

conditions such as sputtering gas medium, substrate temperature and operating pressure were studied. These films were subjected to post-deposition annealing at 600 °C and their properties were investigated. Thermally grown SiO_2 layers on silicon substrates were examined as diffusion barrier layers.

2. Experimental procedure

The planar magnetron sputtering system (described in detail in [8]) used in these investigations was evacuated by a diffusion pump and rotary pump combination which can produce a base pressure of 10^{-7} Torr. It is a dual-magnetron system with one of the magnetrons fitted with a titanium target (diameter, 75 mm) and the other with a stoichiometric Nd–Fe–B target plate. The titanium magnetron acts as a getter pump during deposition to avoid any contamination of the films from oxygen or water vapour [8]. The titanium magnetron was shielded completely to avoid any cross-contamination during deposition of the Nd–Fe–B thin films. The schematic diagram of the system is shown in Fig. 1. Substrates were clamped onto the heater platform quite firmly to achieve good thermal contact between the platform and the substrate. The target-to-substrate distance was fixed at 5 cm throughout these investigations. Prior to deposition, substrates were heated to the deposition temperature and kept at that value for a few hours, to ensure a uniform and equilibrium temperature over the entire substrate surface.

Films were deposited in pure argon and xenon sputter media separately. While argon sputtering was carried out in a dynamic pumping situation, xenon sputtering was done in a static environment mainly because of the higher cost of xenon gas, i.e., in the case of xenon sputtering the baffle was closed and xenon gas was introduced up to the operating pressure. It is believed that xenon cannot be consumed by either titanium or Nd–Fe–B during sputtering and hence the pressure was constant [8, 9]. Xenon sputtering was carried out at only one pressure, 0.2 Pa, while argon sputtering was done in the pressure range 0.2–5 Pa. Simultaneous operation of the titanium magnetron ensured the burial of any residual gas contaminants in the chamber. Films of thicknesses 0.1 and 10 μm were deposited at room temperature and 360 °C separately. At a constant deposition rate (1.5 nm min^{-1}), films of different thicknesses were grown by increasing the deposition time.

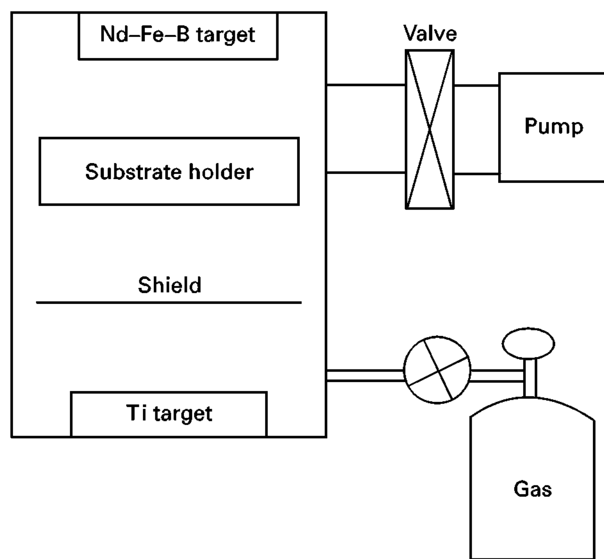

Figure 1 Schematic diagram of the dual-magnetron sputtering system.

Films were also deposited on a silicon substrate with a patterned SiO_2 layer. The SiO_2 layers were grown up to a thickness of 100 Å on Si(100) substrates by oxidizing them using dry thermal oxidation procedures routinely employed in semiconductor processing. This was patterned to open a 5 mm × 5 mm window over silicon such that, in this region, film was directly deposited on the silicon surface while SiO_2 became the base layer elsewhere. This was carried out using standard lithographic techniques. The schematic diagram of the patterned surface is shown in Fig. 2. It facilitates the characterization of the interface of Nd–Fe–B film and silicon and Nd–Fe–B and SiO_2 layers subjected to the same deposition and annealing conditions. These films were subjected to post-deposition heat treatment at a temperature of 600 °C for 20 min in a vacuum of 5×10^{-7} Torr.

The composition and structure of the films were analysed using Rutherford back-scattering spectroscopy (RBS), nuclear reaction analysis (NRA), RBS channelling and selective-area electron diffraction techniques. RBS was carried out using a 2 MeV He^{2+} ion beam in a tandetron accelerator. The composition of the film was determined by using standard simulation methods and comparing it with the experimental Rutherford back-scattering spectrum using the RUMP program [10]. As boron is much lighter than the silicon substrate, it is not possible to determine the boron concentration by the RBS technique alone. Hence, the boron content was obtained from the NRA technique, using the $^{11}B(p,\alpha)^{8}Be$ reaction. This reaction has a cross-section of 100 mb sr^{-1} at $E_p =$ 660 keV [11]. The energy of the incident beam was 660 keV, while the energy of the emitted α particles was 3.4 MeV. A Mylar foil of around 6.5 μm thickness was used to cover the detector to stop the large number of back-scattered protons. A piece of stoichiometric $Nd_2Fe_{14}B$ bulk material was used as the standard. Taking into account the thickness of the film to be analysed and the ranges of the H^+ and α particles, the relative boron concentration was estimated. Initially, the composition of the films (7 μm thick) thicker than the range of both protons and α particles was determined directly comparing it with that of the standard bulk sample. The composition of thinner sample

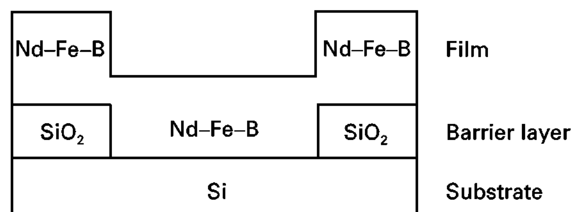

Figure 2 SiO_2 patterned Si substrate.

(1000 Å) was obtained by comparing its NRA spectra with that of the thicker film (7 μm) deposited under the same conditions.

A JEOL 100 kV transmission electron microscope was used for selective-area electron diffraction studies. Mechanical polishing and ion-beam-milling techniques were employed to thin the samples. A special sample holder was used in the electron microscope to facilitate the *in-situ* electron diffraction studies at the pre-set temperature. These studies were carried out while keeping the pre-thinned sample at room temperature and 600 °C.

3. Results and discussion

Fig. 3 shows the typical Rutherford back-scattering spectrum of the film deposited in pure argon at a pressure of 5 Pa, the substrates being kept at room temperature. In this figure, the solid curve represents the experimental data while the open triangles show the simulated spectrum. The composition of the film was estimated to be as follows: Nd, 11.25%; Fe, 68.5%; B, 20.25%. Typical NRA spectra used for the estimation of boron content are shown in Fig. 4. It depicts the NRA spectra of the bulk stoichiometric $Nd_2Fe_{14}B$ as a solid curve, of the 7 μm thick film as open triangles and of the film 1000 Å thick as a broken curve. We believed that this process minimized the uncertainty in the estimation of boron in the film. A similar procedure was followed in determining the composition of the films deposited at different argon pressures. The variation in film composition as a function of operating pressure is shown in Fig. 5. It can be noticed from the figure that the neodymium content was almost constant irrespective of the operating pressure. However, there was a large variation in the composition with respect to the iron and boron concentrations, as the operating pressure was increased. The boron concentration in the films deposited in the complete pressure range (0.2–5 Pa) was found to be much higher than the starting composition in the target. This may be attributed to the relatively lower collision cross-section of the boron atoms (9.4×10^{-20} m^2) compared with the neodymium and iron atoms. However, the observed variation in iron and boron concentration in the film with the change in the operating pressure could be a combined effect of the resputtering of the growing film by the back-scattered energy neutrals and also the loss of sputtered atoms due to gas-phase scattering collisions as the operating pressure was increased.

Fig. 6 shows the channelling spectra of the Nd–Fe–B thin film deposited at the argon pressure of 0.2 Pa on room temperature substrates. From the spectra it is evident that there was no reduction in the yield of the peaks representing neodymium and iron. However, there was considerable reduction in the back-scattered yield from Si substrate. This is a clear indication of the fact that the Nd–Fe–B film still had not formed any texture above the single-crystal silicon substrate. Films deposited at 360 °C also resulted in a similar channelled spectra, indicating the absence of texture in the films. X-ray and electron diffraction analysis of these films showed that the films are amorphous. That means that the films deposited at room temperature and 360 °C in an argon sputter medium are amorphous and did not form any texture.

Channelling studies of the films deposited in a pure xenon sputter medium (0.2 Pa) at ambient substrate temperature (25 °C) also yielded similar spectra to

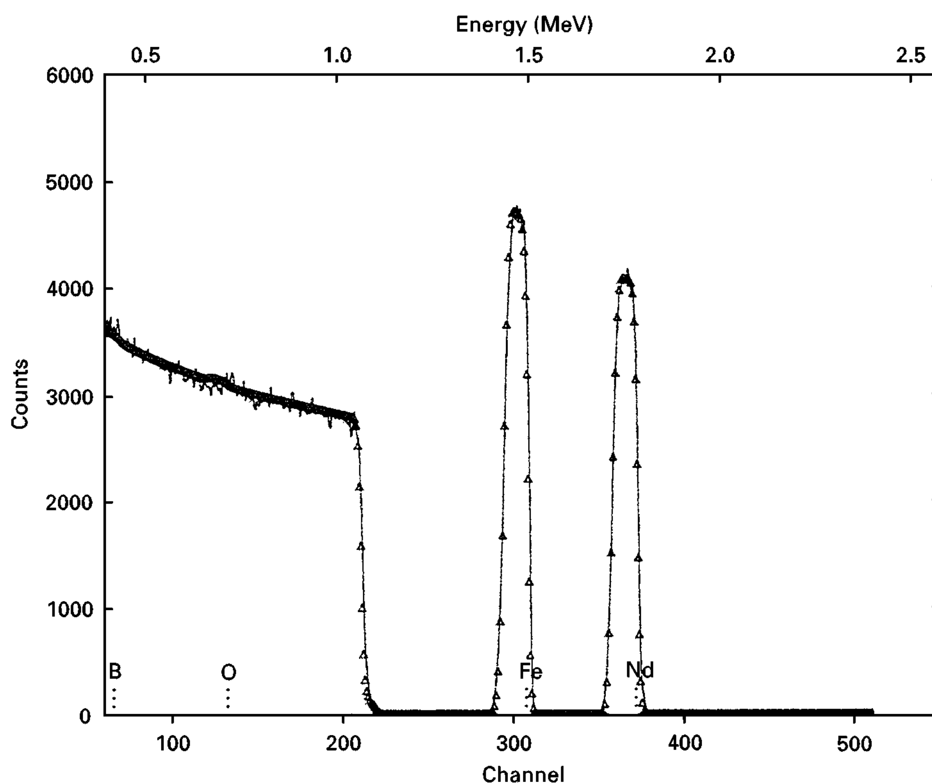

Figure 3 Typical Rutherford back-scattering spectrum of the film deposited at room temperature and an argon pressure of 5 Pa. (—) Experimental spectrum; (△) simulated spectrum to estimate the composition.

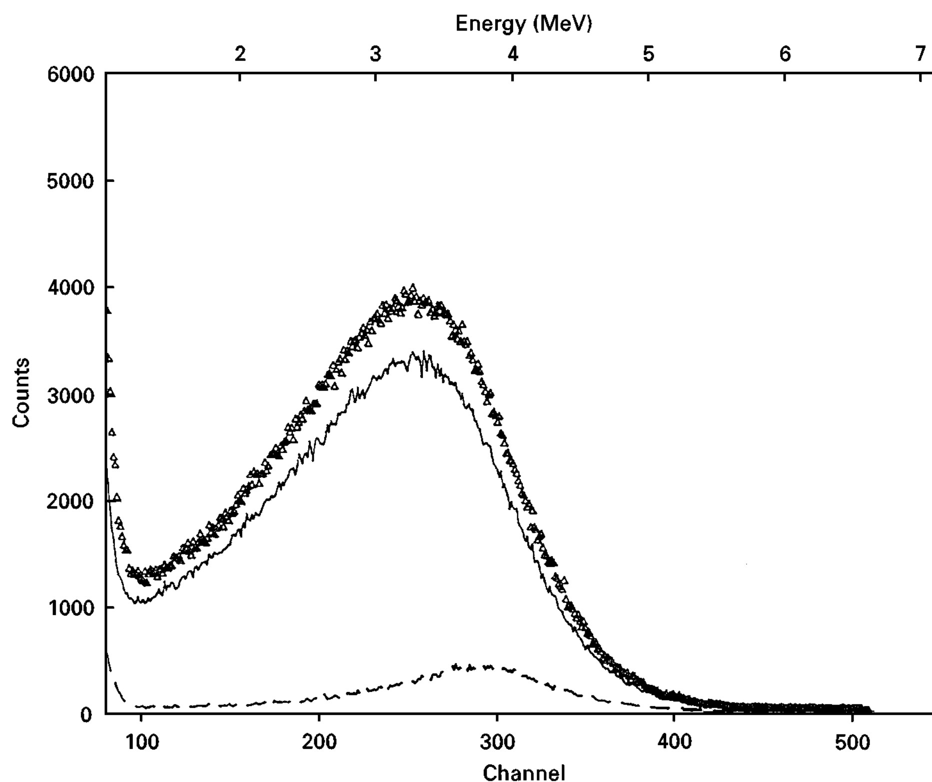

Figure 4 NRA spectra. (—), bulk $Nd_2Fe_{14}B$; (△) film 7 μm thick; (- - -), film 1000 Å thick. Both the films were deposited in the argon sputter medium at room temperature.

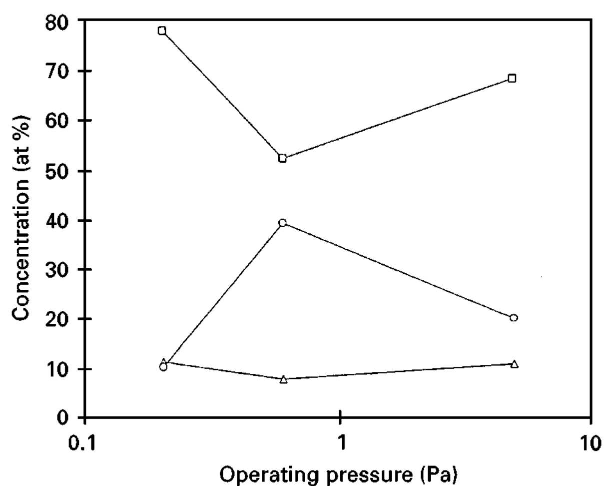

Figure 5 Variation in film composition with operating argon pressure. (△) Nd; (□) Fe; (○) B.

those observed with argon sputter medium. Since these rare-earth–transition-metal systems are known to form amorphous or microcrystalline deposits for substrate temperatures less than 350 °C, the amorphous nature of the films deposited at room temperature irrespective of the sputter medium used is justified. However, the channelled spectra of films deposited at 360 °C at the same xenon pressure is different, as shown in Fig. 7. In this case, the channelled spectra showed a reduction in the minimum yield $\chi_{\min}$ to an extent of almost 50% compared with the random yield, even at the peaks representing the neodymium and iron thicknesses. This can be considered as an indication of the formation of some sort of texture in the Nd–Fe–B film.

From the above data, it is clear that the films deposited in xenon at 360 °C exhibited some texture, while those deposited in pure argon under the same deposition conditions are amorphous. The reason for this behaviour was analysed as follows. One of the major problems encountered whenever a lighter gas and a heavier target combination is used is the high-energy reflected neutral-gas-particle bombardment of the growing film [9]. In this case, as the major part of the target consists of neodymium and iron, which are heavier than the sputter gas argon, the high-energy particle bombardment effects could be significant. To estimate the extent of back-scattering of argon and xenon sputter gas atoms, computations were carried out using TRIM-91. The energy of the sputtered atoms, and the number and energy of the back-scattered atoms were calculated for the argon and xenon atoms incident on the target surface with an energy of 300 eV. These values are listed in Table I. It can be seen from this table that the energies of the sputtered neodymium, iron and boron atoms are higher when sputtered by argon than by xenon for the same incident energy (300 eV). Also, the number of back-scattered particles and their energies are much higher in argon sputtering than in xenon sputtering. Further, calculation of the thermalization distances of sputtered atoms using Westwood's [12] formulation showed that the thermalization distances of the sputtered atoms are comparable with the distance between the target and the substrate at an operating pressure of 0.2 Pa. Thermalization distances of the neodymium, iron and boron in argon sputter media are found to be in the range 6.2–7.5 cm whereas in xenon sputter media it is 5–6 cm, assuming the initial energy of the sputtered atoms to be around 10 eV in both cases. During these calculations, a higher gas temperature (600 K) was included to take the effect of substrate

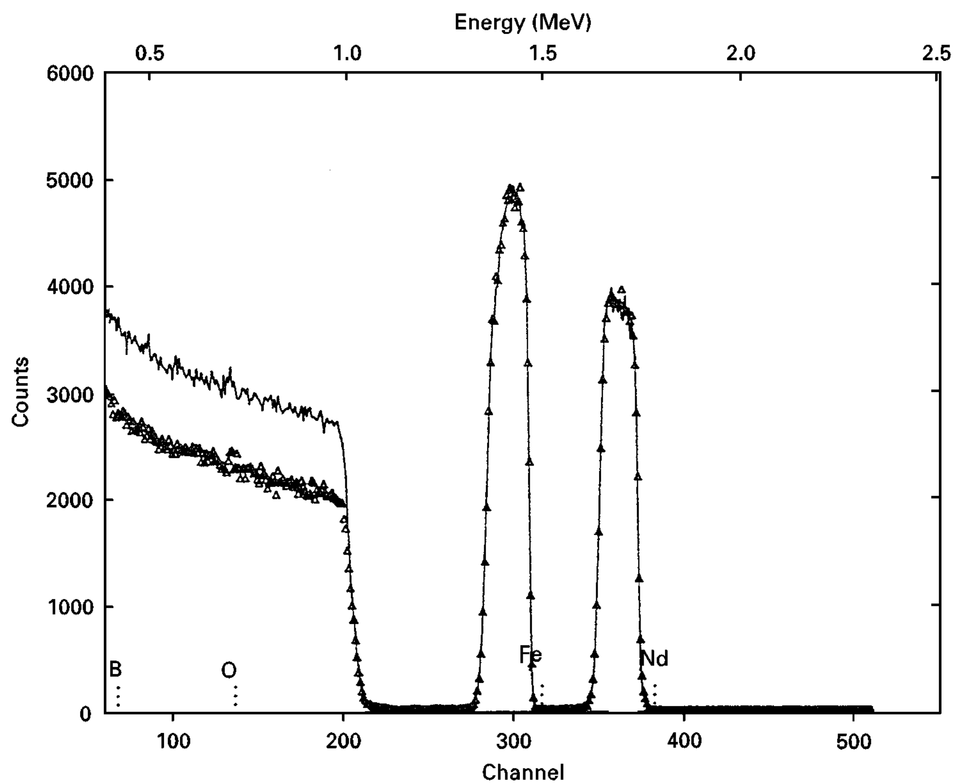

Figure 6 Rutherford back-scattering spectra of the film deposited at room temperature and argon pressure of 0.2 Pa. (—) Random spectrum; (△) channelled spectrum.

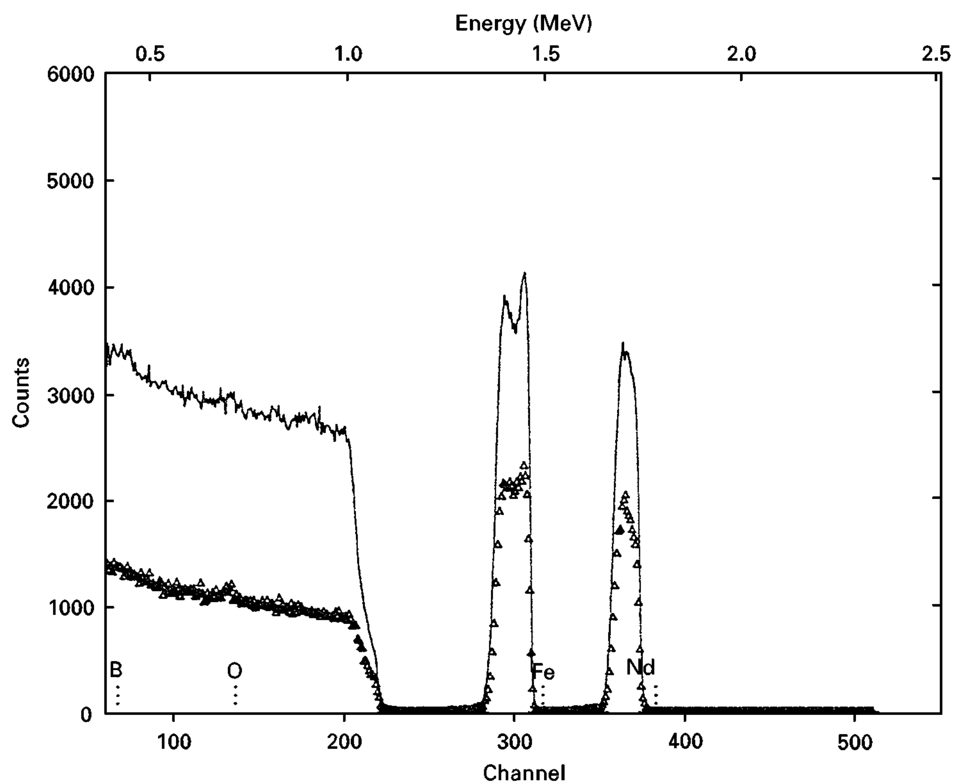

Figure 7 Rutherford back-scattering spectra of the film deposited in the xenon sputter medium at 360 °C. (—) Random spectrum; (△) channelled spectrum.

temperature into account. In the case of argon sputtering, back-scattered gas atoms/particles have an average energy of 30 eV. The thermalization distances of these particles are expected to be far higher than those of sputtered atoms having an initial average energy of 10 eV, i.e. the thermalization distances of these back-scattered particles can be much higher than the target-to-substrate distance. Hence it is expected that the high-energy neutrals bombard the growing film with higher energies, which disrupts the ordered growth of grains. Even the non-thermalized high-energy sputtered atoms (e.g., iron) may distort the growth of certain textures. In this particular case, both these factors could have contributed to affecting the texture

TABLE I Sputtered and back-scattered particles and their energy computed from TRIM

Sputtering gas atom	Initial energy (eV)	Energy of sputtered atoms ($eV\,atom^{-1}$)			Amount of back-scattered particles (%)	Average energy of back-scattered particles (eV)
		Nd	Fe	B		
Argon	300	3	16.8	0.4	8.5	30–50
Xenon	300	0.5	1.7	0.1	0.08	5–7

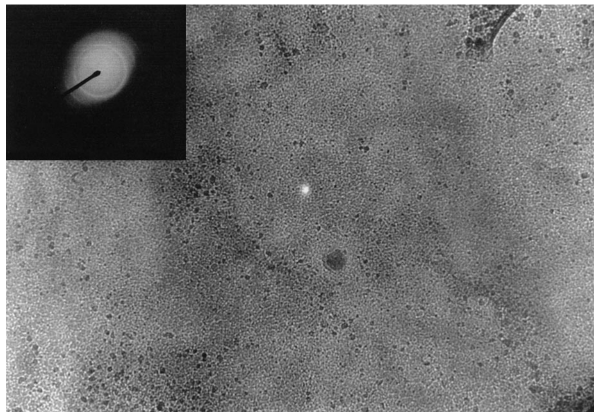

Figure 8 Transmission electron bright-field micrograph of the film deposited in the xenon sputter medium at 360 °C. The inset shows the selected-area diffraction pattern of the same film.

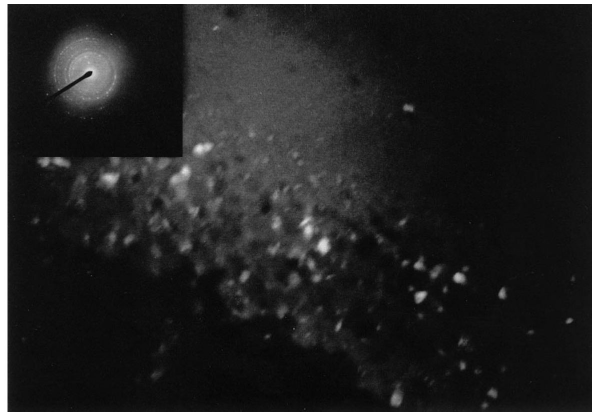

Figure 9 Transmission electron dark-field micrograph of the film deposited in the xenon sputter medium at 360 °C and after annealing to 600 °C (*in-situ* transmission electron microscopy). The inset shows the selected-area diffraction of the same film.

of the growing film, making them amorphous, when deposited in pure argon. A similar observation was made by Cadieu *et al.* [13], during the growth of Sm–Co thin films. On the other hand, these calculations with xenon sputter gas seem to produce very few back-scattered particles. Thermalization distances are also relatively lower in the pure xenon sputter media. As a result, argon-sputtered films appear to be completely amorphous without the formation of any texture, while xenon-sputtered films showed a definite texture.

Fig. 8 shows the microstructure and the corresponding selective-area diffraction pattern of the xenon-sputtered film deposited at 360 °C. The microstructure indicates the presence of small particles which appear to be metallic. The average grain size of these particles appear to be around 200 Å. The diffraction pattern shown in the inset closely matches that of the standard *d* spacings of the body-centred cubic phase of α-Fe. The rings in the pattern starting from the innermost are identified as (1 1 0), (2 0 0), (2 1 1) and (3 1 0), respectively. The diffused bright region at the centre could be an indication of the presence of an amorphous phase, which in this case might be a Nd–Fe–B compound. In the bulk also, when the alloy with the composition of the Nd–Fe–B permanent magnet is cooled from a high temperature, it was reported that firstly iron crystallizes as a primary crystal [14]. The formation of crystalline iron in the present case appears to be analogous to the situation reported in the above reference. The dark-field image of the film heated *in situ* in the electron microscope is shown in Fig. 9 with the electron diffraction pattern as the inset. The high-temperature electron diffraction studies at 600 °C indicated the formation of a $Nd_{4.4}Fe_{77.8}B_{7.8}$ phase. The rings in this pattern are identified to correspond to (2 0 1), (3 0 2), (5 0 0), (6 0 1), (6 4 0) and (5 2 4) planes, respectively, when compared with the standard *d*-values [15]. Interestingly, this tetragonal phase with lattice constants $a = 12.77$ Å and $c = 8.853$ Å was reported to have formed when the amorphous melt-spun ribbons were annealed to 600 °C in vacuum or an inert-gas atmosphere. The formation of this phase in the present investigations after vacuum annealing at 600 °C is in complete agreement with the reported observations in bulk material [15]. The dark-field image shows the presence of small crystallites that are formed during the *in situ* annealing process. The dark field image was taken at the ring representing the (5 0 0) plane.

Fig. 10 shows the Rutherford back-scattering spectra of the film deposited at 360 °C in the xenon sputter medium on silicon in the as-deposited condition (solid curve) and after annealing to 600 °C in vacuum (open triangles). It can be noticed from this spectrum that the change in the portion representing the neodymium thickness (between the channels at around 350–380) after annealing, is relatively small compared with that of iron. In the case of iron, the reduction in the peak height to almost half and at the same time its spread from around 260 to 230 in the lower-energy end of the spectrum is a clear indication of the interdiffusion between iron and silicon. However, it can also be noticed from Fig. 10 that the slope of the line representing the low-energy edge of both neodymium and iron at the interface did not change. The shift of the silicon edge from channel 200 to 220 indicates the presence of silicon on the surface. This is possibly either due to the direct exposure of silicon to the beam through micropores or due to its diffusion

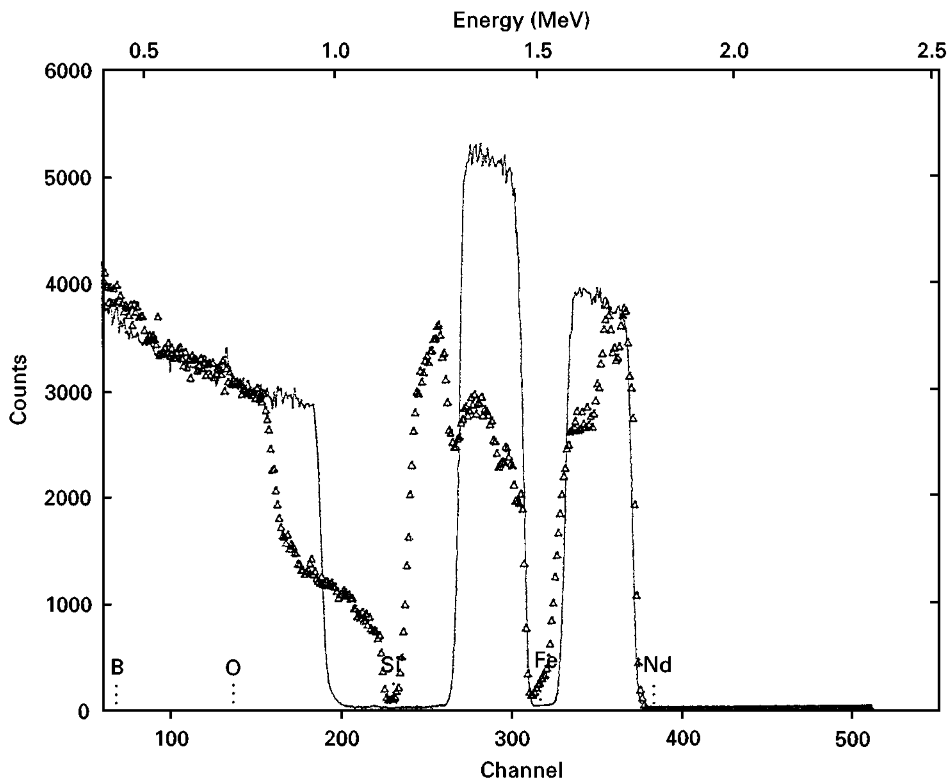

Figure 10 Rutherford back-scattering spectra of the film deposited on silicon in the xenon sputter medium at 360 °C and annealed to 600 °C in vacuum. (—) As deposited, (△) after annealing.

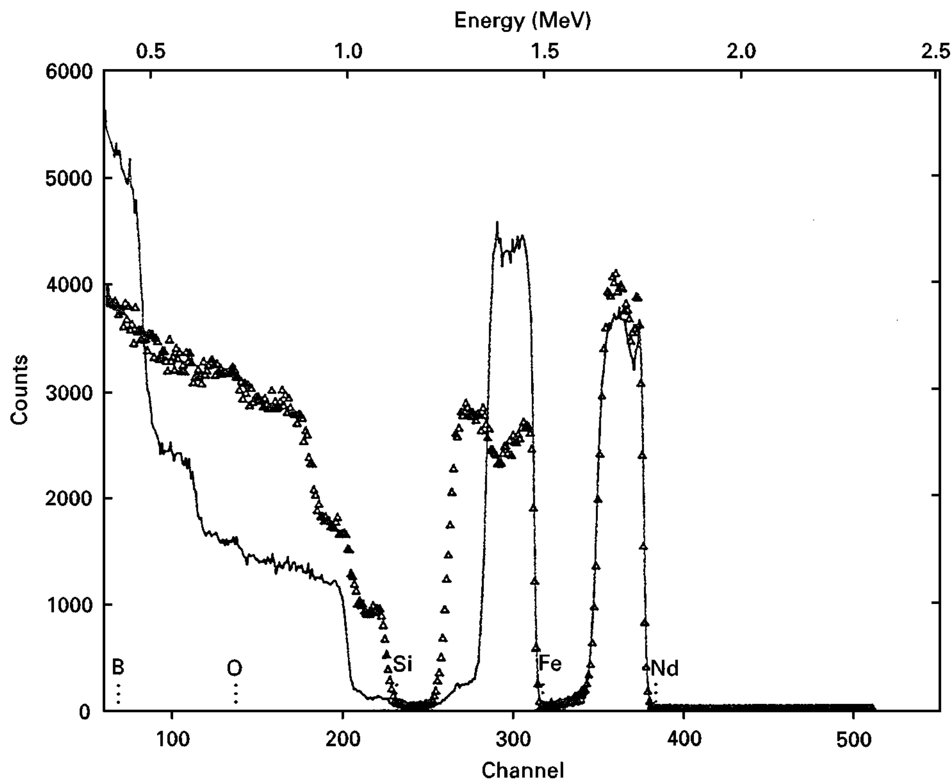

Figure 11 Rutherford back-scattering spectra of the 600 °C vacuum-annealed film deposited on a SiO_2 patterned silicon substrate in the xenon sputter medium at 360 °C. (—) Film deposited on the SiO_2 region; (△) film deposited on the silicon region.

onto the top. However, in the absence of these film–substrate interactions, one can form a Nd–Fe–B phase as was observed with the *in-situ* annealed free-standing ion-beam-thinned transmission electron microscopy sample (Fig. 9). As the temperature required for the formation of iron silicide is around 450–550 °C [16], the probability for such a layer formation is higher when annealed to 600 °C. The efforts to carry out channelling analysis were not successful, indicating the fact that an ordered texture is absent.

Fig. 11 shows the Rutherford back-scattering spectra of the film vacuum annealed to 600 °C, after

deposition at 360 °C on a patterned silicon wafer with SiO_2 layer on the top (as shown in Fig. 2). This film was deposited in the xenon sputter medium. The solid curve and open triangles correspond to two different regions of the same film deposited on silicon and SiO_2, respectively, after annealing. The spectrum of the film region deposited directly on silicon shows a similar trend of film-substrate interaction as was shown in Fig. 10. However, the spectrum representing the film on the SiO_2 region indicates minimal interdiffusion between the film and the substrate. The thickness of the SiO_2 layer in this case is only 100 Å. Probably, a thicker SiO_2 layer may help in completely preventing the interdiffusion. This clearly shows that SiO_2 could be a good choice as a barrier layer to prevent interdiffusion. However, its effect on the Nd–Fe–B film structure and magnetic properties warrant further investigations.

The surface of the films deposited at room temperature and 360 °C was observed by scanning electron microscopy. These films did not show any features and appear to have a smooth surface. A typical scanning electron micrograph of the xenon-sputtered film deposited at 360 °C is shown in Fig. 12a. The surface of the film after post-annealing at 600 °C shows a small grainy structure containing some micropores as shown in Fig. 12b. The film surface indicates the presence of silicon when analysed using energy-dispersive spectroscopy, while no silicon signal was observed on the surface of the film shown in Fig. 12a. This confirms the kind of interdiffusion characteristics observed in the Rutherford back-scattering spectra above. The large dark regions are due to the presence of some dust particles. However, when thicker films (7 μm) were annealed, they exhibited microcracks as shown in Fig. 13. The microcracking observed with thicker films might be due to the large internal stresses developed during post-annealing. The surface of these thicker films before annealing, i.e., in the as-deposited conditions, appeared similar to the thinner films as shown in Fig. 12a. The lattice mismatch between silicon (diamond structure; $a = 5.43$ Å) and $Nd_2Fe_{14}B$ (tetragonal; $a = 8.4$ Å and $c = 12.4$ Å) or $Nd_{4.4}Fe_{77.8}B_{7.8}$ (tetragonal; $a = 12.77$ Å and $c = 8.853$ Å) and the difference between the thermal expansion coefficients (4.68×10^{-6} K^{-1} for silicon and 5.2×10^{-6} and -0.8×10^{-6} K^{-1} in the easy-magnetization and perpendicular directions, respectively, for Nd–Fe–B) could have contributed to these stresses. In addition, the internal stresses in thin films are known to increase with increasing film thickness. All these factors might have resulted in the cracking of the films. A similar cracking was also observed with Sm–Co films thicker than 10–12 μm, when deposited on bare sapphire or polycrystalline substrates, which was attributed to different forms of stresses [6].

The magnetic measurements of the as-deposited films indicated the in-plane magnetic anisotropy with low coercivities. However, further work to improve the magnetic properties is in progress.

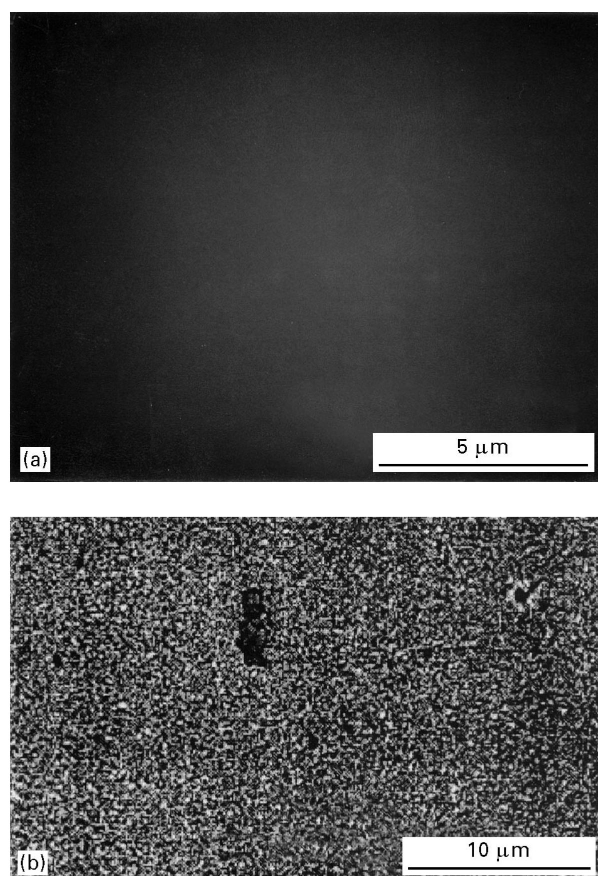

Figure 12 Scanning electron micrograph of the xenon-sputtered film deposited at 360 °C (film thickness, about 1000 Å); (a) as deposited condition; (b) after vacuum annealing to 600 °C.

4. Summary

Nd–Fe–B thin films were deposited on Si(100) at two different substrate temperatures in pure argon and xenon sputter media separately. Films deposited at a substrate temperature of 360 °C in the xenon sputter medium showed the formation of an isolated α-Fe phase with an ordered texture, while those deposited in pure argon were still amorphous. The probable reasons for such variation were explained in terms of the energy of reflected neutrals. Post-deposition annealing in vacuum resulted in interdiffusion between

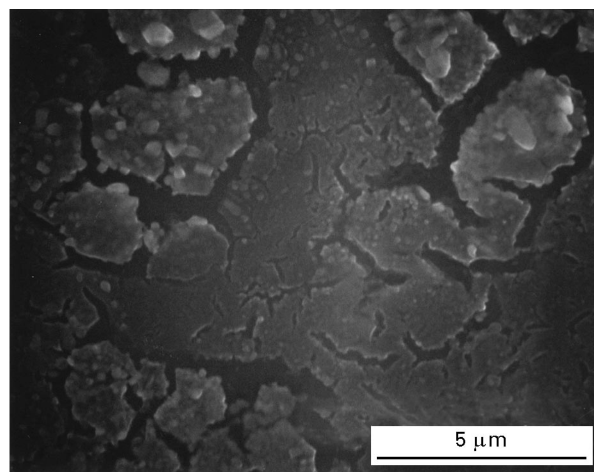

Figure 13 Scanning electron micrograph of the xenon-sputtered film deposited at 360 °C and then subjected to vacuum annealing at 600 °C (film thickness, about 7 μm) (same scale and magnification as the scanning electron micrograph shown in Fig. 12a).

the film and the substrate. Interdiffusion mainly appears to be iron dominated and leads to its segregation from the host material Nd–Fe–B and forms some silicides. However, post annealing of free-standing film in a transmission electron microscope showed the formation of a boron-rich $Nd_{4.4}Fe_{77.8}B_{7.8}$ phase. SiO_2 appears to be a potential candidate as a barrier layer to minimize the interdiffusion between Si and the Nd–Fe–B film.

Acknowledgements

This work was performed under the management of the Micromachine Centre as a part of Industrial Science and Technology Frontier Program 'Research and Development of Micromachine Technology' of Japanese Ministry of International Trade and Industry supported by the New Energy and Industrial Technology Development Organization. The authors thank Profesor Andrew Pogony for useful discussions. The authors also thank Mr Robert Short for his assistance with the tandetron accelerator.

References

1. F. J. CADIEU, *J. Appl. Phys.*, **61** (1987) 4105.
2. K. D. AYLESWORTH, Z. R. ZHAO, D. J. SELLMYER and G. C. HADJIPANAYIS, *ibid.* **64** (1988) 5742.
3. *Idem.*, *J. Magn. Magn. Mater.* **82** (1989) 48.
4. S. YAMASHITA and J. YAMASAKI, M. IKEWDA and N. IWABUCHI, *J. App. Phys.* **70** (1991) 6627.
5. T. ARAKI and OKABE, in Proceedings of the Ninth International Workshop on Microengineering of Electromechanical Systems, San Diego, CA, USA, 11–15 February 1996 (IEEE, New York, 1996) p. 244.
6. F. J. CADIEU, *Phy. Thin Films* **16** (1992) 145.
7. A. NAZARETH, H. D. CHOPRA, D. K. SOOD and R. B. ZMOOD, *Mater. Res. Soc. Symp. Proc.* **354** (1995) 511.
8. B. WINDOW, *J. Vac. Sci. and Technol. A* **11** (1993) 1522.
9. B. WINDOW and G. L. HARDING, *ibid.* **11** (1993) 1447.
10. L. R. DOOLITTLE, *Nucl. Instrum. Methods B* **9** (1985) 344.
11. L. C. FELDMAN and S. T. PICRAUX, in "Ion beam handbook of material analysis", (edited by J. W. Meyer and E. Rimini, Academic Press, New York, 1977) pp. 118, 140.
12. W. D. WESTWOOD, *J. Vac. Sci. Technol.* **15** (1978) 1.
13. F. J. CADIEU, H. HEGDE and K. CHEN, *J. Appl. Phys.* **67** (1990) 4969.
14. M. SAGAWA, S. HIROSAWA, H. YAMAMOTO, S. FUJIMURA and Y. MATSUURA, *Jpn J. Appl. Phys.* **26** (1987) 785.
15. Joint Committee on Powder Diffraction Standards, "Powder diffraction file" (International Center for Diffraction Data, Southmore, PA, 1994) Card 43-1065.
16. F. MOHAMMADI, *Solid State Technol.* **24** (1981) 65.

Received 19 August 1996
and accepted 17 June 1997